Role of the C-terminal domain in inactivation of brain and cardiac sodium channels

Massimo Mantegazza, Frank H. Yu, William A. Catterall, and Todd Scheuer*

Department of Pharmacology, University of Washington, Seattle, WA 98195

Contributed by William A. Catterall, October 22, 2001

Inactivation is a fundamental characteristic of Na^+ channels, and small changes cause skeletal muscle paralysis and myotonia, epilepsy, and cardiac arrhythmia. Brain $Na_v1.2a$ channels have faster inactivation than cardiac $Na_v1.5$ channels, but minor differences in inactivation gate structure are not responsible. We constructed chimeras in which the C termini beyond the fourth homologous domains of $Na_v1.2a$ and $Na_v1.5$ were exchanged. Replacing the C-terminal domain (CT) of $Na_v1.2a$ with that of $Na_v1.5$ ($Na_v1.2/1.5CT$) slowed inactivation at +40 mV ≈2-fold, making it similar to $Na_v1.5$. Conversely, replacing the CT of $Na_v1.5$ with that of $Na_v1.2a$ (Nav1.5/1.2CT) accelerated inactivation, making it similar to $Na_v1.2a$. Activation properties were unaffected. The voltage dependence of steady-state inactivation of $Na_v1.5$ is 16 mV more negative than that of $Na_v1.2a$. The steady-state inactivation curve of $Na_v1.2a$ was shifted +12 mV in $Na_v1.2/1.5CT$, consistent with destabilization of the inactivated state. Conversely, $Na_v1.5/1.2CT$ was shifted −14 mV relative to $Na_v1.5$, consistent with stabilization of the inactivated state. Although these effects of exchanging C termini were consistent with their effects on inactivation kinetics, they magnified the differences in the voltage dependence of inactivation between brain and cardiac channels rather than transferring them. Thus, other parts of these channels determine the basal difference in steady-state inactivation. Deletion of the distal half of either the $Na_v1.2$ or $Na_v1.5$ CTs accelerated open-state inactivation and negatively shifted steady-state inactivation. Thus, the C terminus has a strong influence on kinetics and voltage dependence of inactivation in brain $Na_v1.2$ and cardiac $Na_v1.5$ channels and is primarily responsible for their differing rates of channel inactivation.

Voltage-gated Na^+ channels play an essential role in most excitable cells where they transiently increase the Na^+ conductance in response to membrane depolarization (1). Brain Na^+ channels generate the action potential that is the basis for neuronal electrical excitability. Cardiac Na^+ channels cause the initial depolarization of the cardiac action potential that is responsible for the rapid spread of excitation through the atria and ventricles, generating synchronous cardiac contraction.

The principal component of the voltage-gated Na^+ channel is a 260-kDa α subunit, which forms the pore and is responsible for the voltage-sensitive properties of the channel (2–4). The primary sequence of the α subunit contains four homologous domains (I–IV) each containing six transmembrane α-helices (S1–S6) as well as a segment connecting S5 and S6 of each domain that forms the narrow outer end of the ion-conducting pore.

Na^+ channels respond to membrane depolarization by activating, opening, allowing Na^+ current to flow, and then rapidly inactivating. Fast inactivation is a fundamental property of Na^+ channels, and minor modifications cause inherited skeletal muscle myotonia and paralysis, cardiac arrhythmia, and epilepsy (5, 6). $Na_v1.2a$, a principal Na^+ channel isoform in adult brain (7, 8), has faster inactivation kinetics and more positive voltage dependence of inactivation than the cardiac $Na_v1.5$ channel (9).

The fast inactivation gate is formed by the intracellular loop between domains III and IV (10–12), which blocks the ion conducting pore a few milliseconds after the channel opens (13). However, replacement of the $Na_v1.5$ inactivation gate with that of $Na_v1.2a$ does not transfer the inactivation properties (14). Therefore, the molecular determinants governing these inactivation properties must lie elsewhere in the channel.

One possible location is the C-terminal domain (CT) of the α subunit beyond segment IVS6. Multiple mutations that cause human diseases related to inactivation have been identified in the CT of the cardiac sodium channel (15–20). In these experiments, we have studied chimeric channels exchanging $Na_v1.2a$ and $Na_v1.5$ C termini. Substituting only the CT transferred inactivation kinetics from one channel to the other and had additional major effects on the voltage dependence of steady-state inactivation. Further analysis using truncated brain and heart channels indicated that the distal half of the CT of both channels inhibited inactivation. Overall, our findings indicate that the CT plays a critical role in inactivation and is responsible for the differences in inactivation rate between cardiac and brain Na^+ channels.

Experimental Procedures

Construction of Chimeras and Mutagenesis. Plasmid, pCDM8-rH1, encoding the cardiac $Na_v1.5$ α subunit, has been described (21). Plasmid pCDM8-rIIA encoding the $Na_v1.2a$ α subunit (22) contains a unique, silent *Xho*I restriction site at the junction between IVS6 and the C-terminal cytoplasmic region (amino acid positions L1776–E1777). An equivalent restriction site is present in pCDM8-rH1. Chimeric Na^+ channels were constructed by exchanging a restriction fragment between this *Xho*I site and a vector *Cla*I site including the entire CT of $Na_v1.2a$ and $Na_v1.5$ Na^+ channels. The resulting chimeric channels $Na_v1.2$-E1777-$Na_v1.5$-E1775CT and $Na_v1.5$E1775-$Na_v1.2$E1777CT were designated $Na_v1.2/1.5CT$ and $Na_v1.5/1.2CT$, respectively. The truncation mutations deleting segments of the CT of the $Na_v1.2a$ channel α subunit were constructed by standard PCR mutagenesis by insertion of a stop codon. Mutagenic oligonucleotides were designed in reverse orientation with an in-frame TAA stop codon followed by *Cla*I restriction site; the forward oligonucleotide was designed from sequences in the IVS6 transmembrane segment, upstream of the *Xho*I site. The PCR fragments were each digested with *Xho*I and *Cla*I and subcloned into the identical sites of pCDM8-rIIA. This procedure yielded the truncated $Na_v1.2a$ channel constructs $Na_v1.2\Delta E1777$, $Na_v1.2\Delta K1863$, $Na_v1.2\Delta I1877$, $Na_v1.2\Delta K1890$, $Na_v1.2\Delta A1909$, $Na_v1.2\Delta S1929$, $Na_v1.2\Delta T1951$, $Na_v1.2\Delta S1977$, and $Na_v1.2\Delta K1998$.

Cell Culture and Transfection. The tsA-201 cell subclone of HEK293 cells was maintained as described (23). The plasmid containing cDNA for the Na^+ channel was cotransfected with pIRES-EYFP (CLONTECH) encoding the yellow variant of green fluorescent protein by $CaPO_4$ precipitation as described (24). Twelve hours after transfection, the cells were replated at

Abbreviation: CT, C-terminal domain.

*To whom reprint requests should be addressed. E-mail: scheuer@u.washington.edu.

The publication costs of this article were defrayed in part by page charge payment. This article must therefore be hereby marked "*advertisement*" in accordance with 18 U.S.C. §1734 solely to indicate this fact.

www.pnas.org/cgi/doi/10.1073/pnas.211563298

low density for electrophysiological recordings. Transfected cells were identified by fluorescence.

Electrophysiology and Data Analysis. Whole-cell patch-clamp recordings were performed at room temperature by using an Axopatch 200B amplifier (Axon Instruments, Union City, CA) with PCLAMP 6 software (Axon Instruments). Capacitative currents were minimized by using the amplifier circuitry. Seventy percent prediction and 90–95% series resistance compensation were routinely used. Remaining linear capacity and leakage currents were eliminated by P/4 subtraction. The intracellular solution contained 120 mM CsAspartate, 5 mM NaCl, 2 mM $MgCl_2$, 10 mM EGTA, 10 mM Hepes, pH 7.3 with CsOH. The extracellular solution contained 140 mM NaCl, 2 mM $CaCl_2$, 2 mM $MgCl_2$, 10 mM Hepes, pH 7.4 with NaOH. Current signals were filtered at 5 or 10 kHz before sampling.

Conductance-voltage (g-V) relationships (activation curves) were calculated from the current-voltage (*I–V*) relationships according to $g = I_{Na}/(V - E_{Na})$, where I_{Na} was the peak Na^+ current measured at potential, V, and E_{Na}, the calculated equilibrium potential.

Normalized activation and inactivation curves were fit to Boltzmann relationships of the form: $y = 1/\{1 + \exp[(V - V_{1/2})/k]\} + A$, where y is normalized g_{Na} or I_{Na}, A, the baseline, V, the membrane potential, $V_{1/2}$, the voltage of half-maximal activation, V_a, or inactivation, V_h, and k is a slope factor. In fitting the activation curves, A was fixed at 0. Inactivation kinetics were evaluated by fitting the decay of the current from the peak to a point 60 ms from the beginning of the voltage stimulus, with the sum of two exponentials and a baseline. Statistical results are given as mean ± SEM. Statistical analyses were performed by using PRISM 3 (GraphPad, San Diego) software. The threshold P value for statistical significance was 0.05.

$Na_v1.2a$ and its mutants generate a variable amount of persistent Na^+ current in different transfected cells, which was not observed for $Na_v1.5$ and its mutants (25).† Only cells with less than 8% persistent current were selected for analysis to permit comparison with $Na_v1.5$.

Results

Inactivation of Na^+ Channels from Closed and Open States. After strong depolarization, Na^+ channels are thought to move through a series of closed states (Cn; Scheme 1), reach the open

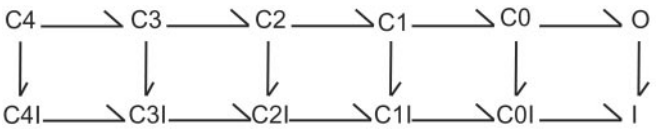

state (O), and rapidly inactivate (I).

These state changes are driven by voltage-dependent movement of gating charges in the channel structure. At positive membrane potentials, Na^+ channels rapidly open and the rate of decay of the Na^+ current reflects the inactivation of open channels (O → I). For weaker depolarizations, Na^+ channels transit rightward through the series of close states (Cn) but usually inactivate by transition into one of the CnI states before opening (Scheme 1), causing steady-state inactivation. The molecular transitions governing rapid inactivation from the open state and slower, steady-state inactivation from closed states are distinct (Scheme 1), and we show below that the CT affects these aspects of inactivation differentially.

†Mantegazza, M. A., Yu, F., Catterall, W. A. & Scheuer, T. (2000) *Biophys. J.* **78,** 88A (abstr.).

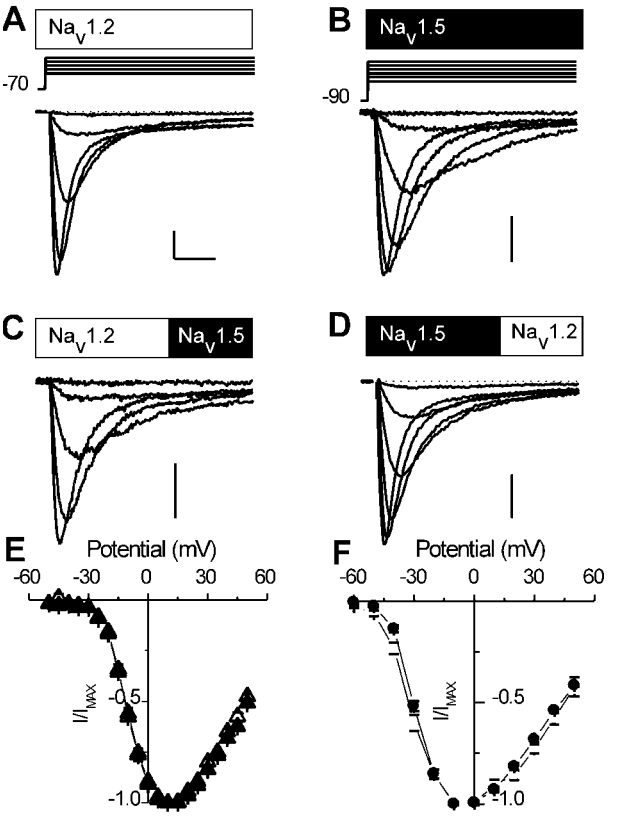

Fig. 1. Na^+ currents in tsA-201 cells transfected with wild-type $Na_v1.2a$, $Na_v1.5$, or chimeric Na^+ channels. (*A–E*) Na^+ current traces recorded in response to depolarizations to the indicated voltages from representative cells transfected with either brain $Na_v1.2a$ α subunits (*A*), cardiac $Na_v1.5$ α subunits (*B*), $Na_v1.2/1.5CT$ chimeric α subunits (*C*), or $Na_v1.5/1.2CT$ chimeric α subunits (*D*). Traces were obtained in response to stimuli at 10-mV intervals as indicated by the voltage protocols above each column. Calibration bars: 1 nA, 3 ms. (*E*) Mean normalized current-voltage (*I–V*) curves for $Na_v1.2a$ (▲; $n = 9$) and $Na_v1.2/1.5CT$ (△, $n = 11$). (*F*) Mean normalized *I–V* curves for $Na_v1.5$ (●, $n = 7$) and $Na_v1.5/1.2CT$ (○, $n = 6$). Chimeric channels generated smaller Na^+ currents than the parental channels. Mean current densities were: $Na_v1.2a$, 550 ± 50 pA/pF ($n = 46$); $Na_v1.2/1.5CT$, 310 ± 50 pA/pF ($n = 15$); $Na_v1.5$, 300 ± 100pA/pF ($n = 7$); $Na_v1.5/1.2CT$, 140 ± 40 pA/pF ($n = 7$).

Substitution of the CTs Does Not Alter the Voltage Dependence of Activation. The activation properties of $Na_v1.2a$ (rIIA; refs. 26 and 27) and $Na_v1.5$ (rH1; refs. 28–30) channels transiently expressed in tsA-201 cells are compared in Fig. 1. $Na_v1.2a$ currents activate positive to −30 mV and peak near +10 mV (Fig. 1 *A* and *E*). $Na_v1.5$ currents activate at more negative potentials. They are first detectable at −50 mV and peak near −10 mV (Fig. 1 *B* and *F*).

To examine the role of the CT, we constructed chimeras between $Na_v1.2a$ and $Na_v1.5$ in which the CTs of the channels were exchanged. In $Na_v1.2/1.5CT$, the $Na_v1.5$ CT, beginning with E1775, replaced the CT of $Na_v1.2a$, which had been truncated before E1777. In $Na_v1.5/1.2CT$, the $Na_v1.2a$ tail from E1777 replaced the CT of the $Na_v1.5$ channel, beginning with the E1775. The voltage dependence of activation was unaffected in either chimeric channel, indicating that the CT is not responsible for the markedly different voltage dependence of activation of the $Na_v1.2a$ and $Na_v1.5$ channels.

To examine the differences in Na^+ current time course more closely, mean Na^+ currents from the wild-type and chimeric channels were compared (Fig. 2*A*). The $Na_v1.5$ channel activates more slowly than the $Na_v1.2a$ channel, even at the strongly positive potential of +40 mV. These differing activation kinetics were

NEUROBIOLOGY

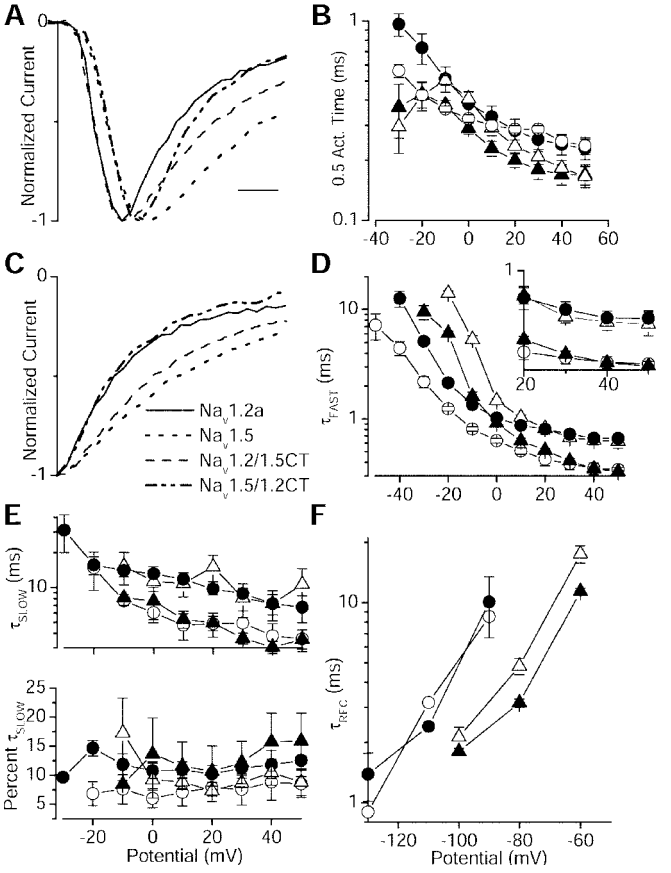

Fig. 2. Kinetics of the Na^+ current. (*A*) Averages of current traces at +40mV for each channel type. (*B*) Semilogarithmic plot of times of half activation at the indicated potentials for $Na_v1.2a$ (▲; $n = 8$), $Na_v1.2/1.5CT$ (△; $n = 9$), $Na_v1.5$ (●; $n = 7$), and Nav1.5/1.2CT (○; $n = 5$). (*C*) Traces from *A* shifted in time so that their peaks are aligned to allow a direct comparison of inactivation kinetics. (*D* and *E*) Parameters derived from fits of the sum of two exponential functions to the decay of the current traces during depolarizations to the indicated potentials. Semilogarithmic plot of the voltage dependence of τ_{Fast} (*D*), τ_{Slow} (*E Upper*), and fraction of the decay represented by τ_{Slow} (*E Lower*). (*D Inset*) Replot of the time constants between +20 and +50 mV on a linear scale. (*F*) Time constants for recovery from inactivation at the indicated potentials. The points for $Na_v1.5/1.2CT$ were obtained from a single cell because of difficulties in expressing that construct.

unaffected when the CT tail was replaced by that of the other channel. This finding was confirmed at a range of potentials by measuring the time to half activation (Fig. 2*B*). At all positive potentials, the time to half activation was determined by the identity of the parental channel rather than by the identity of the CT.

The CT Determines the Kinetics of Inactivation. $Na_v1.2a$ currents decay faster than $Na_v1.5$ currents (compare Fig. 1 *A* and *B*). In contrast to the lack of effect on activation, substitution of the $Na_v1.5$ tail in the $Na_v1.2a$ channel slowed the decay of the current (compare Fig. 1 *A* and *C*). The converse effect is observed in $Na_v1.5/1.2CT$, which has faster inactivation than the parental $Na_v1.5$ channel (compare Fig. 1 *B* and *D*).

Whereas $Na_v1.5$ and the $Na_v1.5/1.2CT$ activate with identical kinetics (Fig. 2 *A* and *B*), the two traces diverge at the peak with the $Na_v1.5/1.2CT$ current decaying significantly more rapidly than $Na_v1.5$. Similarly, $Na_v1.2/1.5CT$ inactivates more slowly than $Na_v1.2a$. These effects are seen clearly when the peaks of the current traces are aligned so that inactivation kinetics can be compared directly (Fig. 2*C*). $Na_v1.5/1.2CT$ inactivates with the kinetics of the $Na_v1.2a$ channel. $Na_v1.2/1.5CT$ inactivates with the kinetics of the $Na_v1.5$ channel. To quantify its time course, current decay was fit with the sum of two exponential components (Fig. 2 *D* and *E*). Although the second, slower exponential was required, >80% of the decay was described by the faster exponential component (Fig. 2*E*). The $Na_v1.2/1.5CT$ channel inactivates more slowly than the parental $Na_v1.2a$ channel at all potentials, whereas the $Na_v1.5/1.2CT$ channel inactivates more rapidly than the parental $Na_v1.5$ channel at all potentials (Fig. 2*D*). In addition, at potentials positive to +20 mV the time constant of Na^+ current decay became identical to that of the channel from which the CT was derived (Fig. 2*D Inset*). At these positive potentials current decay reflects inactivation of open channels (Scheme I) and the differences in inactivation kinetics are determined entirely by the CT. The slow time constants were also determined by the identity of the CT (Fig. 2*E*). Thus, the isoform-specific rates of inactivation of open channels are determined primarily by the identity of the CT for $Na_v1.2a$ and $Na_v1.5$.

Recovery from Inactivation Is Unaffected by the Identity of the CT. We also determined the rate of recovery from inactivation. Interestingly, recovery from inactivation was unaffected by exchange of the CTs (Fig. 2*F*).

The CT Modifies the Voltage Dependence of Steady-State Inactivation. A large difference between the voltage dependence of inactivation of the $Na_v1.2a$-derived channels ($Na_v1.2a$ and $Na_v1.2/1.5CT$) and the $Na_v1.5$-derived channels ($Na_v1.5$ and $Na_v1.5/1.2CT$) is expected because of the difference in voltage dependence of activation (Figs. 1 *E* and *F* and 3). The voltage dependence of steady-state inactivation is set by multiple factors, including the rate and stability of the inactivation process. Thus, most mutations that slow inactivation from the open state also cause a positive shift in steady-state inactivation (e.g., refs. 31 and 32). Consistent with this finding, when the CT of $Na_v1.2a$ is substituted for that of $Na_v1.5$ in $Na_v1.5/1.2CT$, the faster rate of inactivation is accompanied by a shift of steady-state inactivation toward more negative potentials, from -60.5 ± 0.2 mV to -75.7 ± 0.1 mV (Fig. 3). Conversely, steady-state inactivation of the $Na_v1.2a$ channel shifts to more positive potentials, from -44.1 ± 0.2 mV to -32.4 ± 0.3 mV, when the $Na_v1.5$ CT is substituted in $Na_v1.2/1.5CT$. Thus, steady-state inactivation of $Na_v1.2a$ from closed states is weakened by substitution of the CT of $Na_v1.5$, and steady-state inactivation of $Na_v1.5$ is strengthened by substitution of the $Na_v1.2a$ CT. The identity of the CT also determines the slope of the inactivation curve, which is shallower for $Na_v1.5$ than for $Na_v1.2a$ channels (Fig. 3). These effects parallel the changes in rates of inactivation of these chimeras from the open state (Figs. 1 and 2). Despite this parallel, the large initial differences in the voltage dependence of steady-state inactivation between the channel isoforms are only increased by exchanging the C-terminal tails, becoming more negative in $Na_v1.5/1.2CT$ and more positive in $Na_v1.2/1.5CT$. This finding indicates that molecular features of these two channel types other than the CT and the inactivation gate itself are dominant determinants of the voltage dependence of steady-state inactivation.

The Distal CTs of $Na_v1.2a$ and $Na_v1.5$ Inhibit Inactivation. The studies with chimeric channels define the effects of the CTs of the $Na_v1.2a$ and $Na_v1.5$ channels relative to each other but they do not reveal the nature of the effect of the Na^+ channel CT *per se*. To obtain this type of information, the simplest experiment would be to delete the CT entirely, thereby removing its influence. However, truncation of $Na_v1.2a$ at E1777 produced a channel that did not give rise to detectable currents. Smaller truncations at K1863 and I1877 gave rise to Na^+ currents too

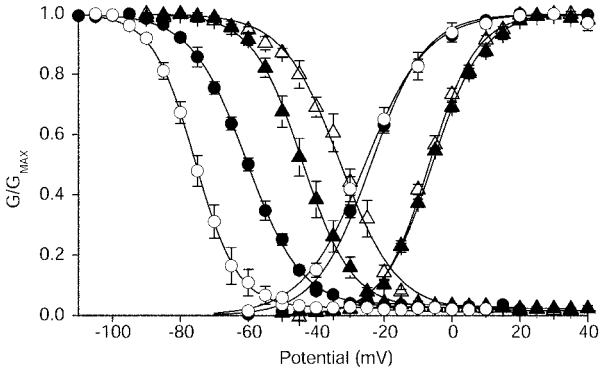

Fig. 3. Voltage dependence of activation and inactivation. Mean voltage dependence of activation and inactivation for $Na_v1.2a$ (▲), $Na_v1.2/1.5CT$ (△), $Na_v1.5$ (●), and $Na_v1.5/1.2CT$ (○). For $Na_v1.2a$ and $Na_v1.2/1.5CT$ the inactivation protocol used a test pulse to 0 mV, preceded by 100-ms long prepulses to the indicated potentials. The holding potential was −100 mV. For $Na_v1.5$ and $Na_v1.5/1.2CT$ the test potential was −20 mV and the holding potential was −120 mV. The continuous lines are mean Boltzmann fits to the individual experiments with the following mean parameters: Activation—$Na_v1.2a$ (n = 9), $V_a = -5.9 \pm 0.5$, $k = 7.2 \pm 0.3$; $Na_v1.2/1.5CT$ (n = 11), $V_a = -6.7 \pm 0.6$, $k = 6.8 \pm 0.3$; $Na_v1.5$ (n = 11), $V_a = -25.9 \pm 1.0$, $k = 7.6 \pm 0.3$; $Na_v1.5/1.2CT$ (n = 8), $V_a = -23.7 \pm 1.9$, $k = 9.0 \pm 0.5$; Inactivation—$Na_v1.2a$ (n = 7), $V_h = -43.9 \pm 1.7$, $k = 6.8 \pm 0.3$; $Na_v1.2/1.5CT$ (n = 10), $V_h = -32.6 \pm 1.5$, $k = 8.1 \pm 0.3$; $Na_v1.5$ (n = 7), $V_h = -60.4 \pm 0.8$, $k = 8.4 \pm 0.3$; $Na_v1.5/1.2CT$ (n = 6), $V_h = -75.1 \pm 1.6$, $k = 6.3 \pm 0.5$. ANOVA followed by Tukey's post test showed that the activation $V_{1/2}$ and k values for the $Na_v1.2a$-derived channels differed from those of the $Na_v1.5$-derived channels. The k value for $Na_v1.5/1.2CT$ differed significantly from the k values for the other constructs. For inactivation curves, the $V_{1/2}$ values for all constructs differed significantly. The inactivation curve k values of $Na_v1.2a$ and $Na_v1.5/1.2CT$ were similar to each other and significantly different from $Na_v1.5$ or $Na_v1.2/1.5CT$.

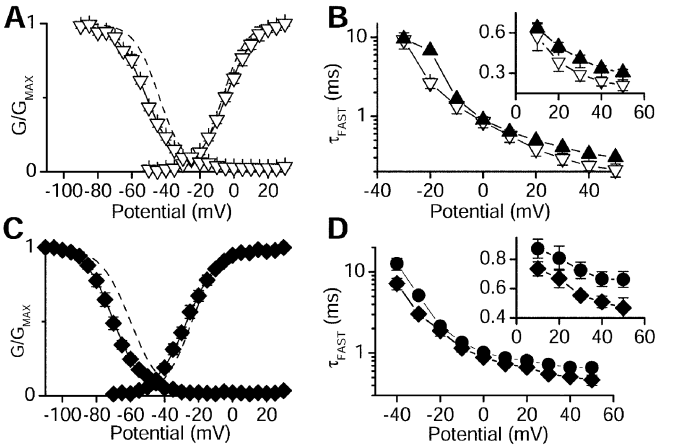

Fig. 4. Properties of the deletion mutants $Na_v1.2\Delta K1890$ and $Na_v1.5\Delta K1888$. (*A*) Mean voltage dependence of activation and inactivation for $Na_v1.2\Delta K1890$ (▽) and $Na_v1.2a$ (dashed lines; from Fig. 3). The mean parameters for Boltzmann fits to individual $Na_v1.2\Delta K1890$ experiments were: $V_a = -4.6 \pm 0.2$ mV, $k = 8.2 \pm 0.1$ mV (n = 7); $V_h = -51.4 \pm 0.3$ mV, $k = 8.6 \pm 0.2$ mV (n = 6). (*B*) Semilogarithmic plot of the fast time constants derived from fits of two exponentials to the decay of the current. (*Inset*) The data for positive potentials on a linear scale. $Na_v1.2a$, ▲; $Na_v1.2$-ΔK1890 (▽). (*C*) Mean voltage dependence of activation and inactivation for $Na_v1.5\Delta K1888$ (◆) and $Na_v1.5$ (dashed lines; from Fig. 3). Fits to $Na_v1.5\Delta K1888$ individual experiments yielded the following mean parameters: $V_a = -26.9 \pm 0.2$, $k = 9.2 \pm 0.2$ (n = 9); $V_h = -70.2 \pm 0.2$, $k = 8.1 \pm 0.2$ (n = 8). (*D*) The fast time constants of two exponential fits to test pulses to the indicated potentials are plotted versus test pulse voltage for $Na_v1.5$ (●) and $Na_v1.5\Delta K1888$ (◆) as in *B*.

small to distinguish from endogenous currents that are sometimes observed in tsA-201 cells (33, 34).

The channel with the largest C-terminal deletion that produced adequate Na^+ currents for analysis was $Na_v1.2\Delta K1890$. Although the activation curve of $Na_v1.2\Delta K1890$ did not differ from $Na_v1.2$, the inactivation curve was shifted −7.3 mV (Fig. 4*A*). Inactivation was more likely at each potential. Inactivation during depolarizations also was faster. The fast time constant for inactivation of $Na_v1.2\Delta K1890$ became significantly faster than $Na_v1.2a$ at potentials more positive than +10 mV (e.g., 1.4-fold at +40 mV; Fig. 4*B Inset*). The equivalent deletion of the CT of $Na_v1.5$ ($Na_v1.5\Delta K1888$; Fig. 4*D*) also had an unchanged activation curve (Fig. 4*C*), but the steady-state inactivation curve was shifted −9.7 mV relative to $Na_v1.5$. Inactivation of $Na_v1.5\Delta K1888$ was also accelerated (1.3-fold at +40 mV; Fig. 4*D*). Because truncating either $Na_v1.2a$ at K1890 or $Na_v1.5$ at the equivalent K1888 enhances inactivation, the C-terminal tail distal to this point normally inhibits inactivation.

Effects of Progressive Deletions of the Distal CT of $Na_v1.2a$ on Inactivation. To localize the molecular determinants of inactivation in the distal CT, we made a series of channels that were truncated C terminal to K1890 (Fig. 5*A*). All generated Na^+ currents similar in magnitude to $Na_v1.2a$. As expected from the results with the larger truncations, effects on the voltage dependence of activation were small for all constructs except $Na_v1.2\Delta S1929$, which produced a substantial negative shift of activation (Fig. 5*A Center*).

In contrast to activation, each deletion mutation produced a significant negative shift of steady-state inactivation in comparison to wild-type $Na_v1.2a$. Surprisingly, the shifts in inactivation did not decrease monotonically with smaller deletions (Fig. 5*A Right*). Instead, a negative shift of inactivation was observed when only the last 8 aa were deleted in $Na_v1.2\Delta K1998$. This pattern suggests at least two loci in the distal CT that affect inactivation—one between residues 1890 and 1951 and one at the extreme CT between residues 1998 and 2005. Because both activation and inactivation are negatively shifted for $Na_v1.2\Delta 1929$, the additional amino acid residues having specific effects on inactivation are likely to be located between residues 1890 and 1929. The effects of deletion of the last eight C-terminal residues are apparently increased by additional deletion of residues 1890–1929.

Na^+ currents through the mutant channels also decayed more rapidly than wild type at all potentials (Fig. 5*B*). This is particularly evident at positive potentials, where the effects of activation rate on inactivation are minimal, as illustrated by the time constants plotted on a linear scale in Fig. 5*B Inset*. The rank orders of the negative shifts in inactivation curves (Fig. 5*A*) and the speeding of inactivation (Fig. 5*B*) are approximately correlated, except for $Na_v1.2\Delta 1909$ and $Na_v1.2\Delta 1951$. Overall, these results show that the CT of $Na_v1.2a$ can selectively inhibit the inactivation, without consistent effects on activation. The effects on inactivation from open states during strong depolarizations and the effects on inactivation from closed states during weaker depolarizations may be affected differently by molecular determinants in the C-terminal tail, as considered in *Discussion*.

Discussion

The CT Has Minimal Effect On Activation. Our results show that the overall CT of the Na^+ channel has no detectable effect on activation. Neither exchange of the CTs between $Na_v1.2a$ and $Na_v1.5$ nor deletion of the distal CT of $Na_v1.2a$ had systematic effects on the kinetics or voltage dependence of channel activation. Because activation is initiated by outward movement of the S4 voltage sensors, it is not surprising that the intracellular CT has little effect.

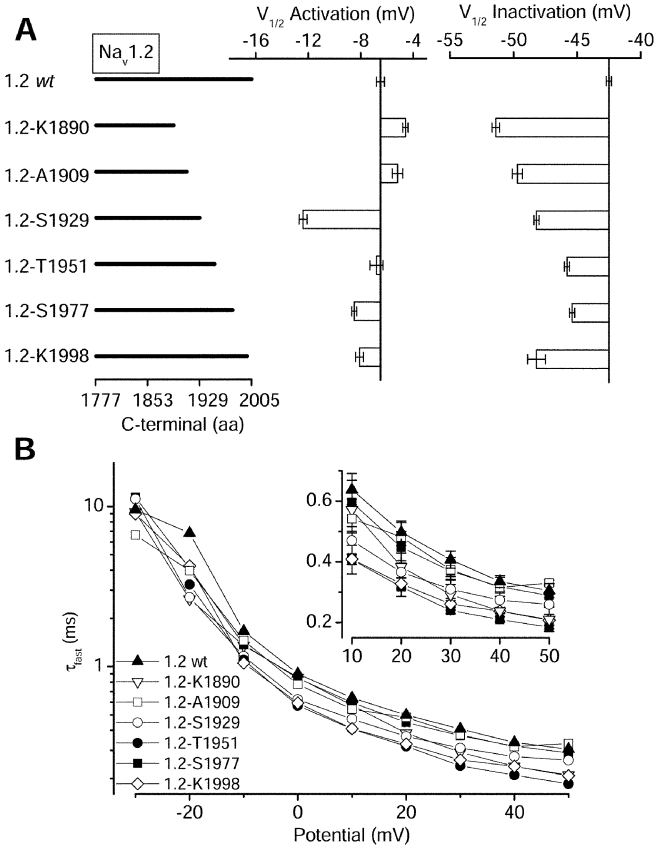

Fig. 5. Voltage-dependent properties of Na$_v$1.2a deletion mutants. (*A*) Bar graphs showing the mean values of the midpoint of the activation (*Center*) and inactivation (*Right*) curves for Na$_v$1.2a ($V_a = -5.9 \pm 0.5$ mV, $n = 9$; $V_h = -43.9 \pm 1.7$ mV, $n = 7$), Na$_v$1.2 ΔK1890 ($V_a = -4.6 \pm 0.2$, $n = 7$; $V_h = -51.4 \pm 0.3$, $n = 6$), Na$_v$1.2-ΔA1909 ($V_a = -5.2 \pm 0.4$, $n = 10$; $V_h = -49.7 \pm 0.4$, $n = 6$), Na$_v$1.2ΔS1929 ($V_a = -12.4 \pm 0.3$, $n = 6$; $V_h = -48.2 \pm 0.2$, $n = 6$); Na$_v$1.2-ΔT1951 ($V_a = -6.8 \pm 0.5$, $n = 9$; $V_h = -48.5 \pm 0.2$, $n = 8$); Na$_v$1.2-ΔS1977 ($V_a = -8.5 \pm 0.2$, $n = 13$; $V_h = -45.4 \pm 0.2$, $n = 10$), and Na$_v$1.2ΔS1998 ($V_a = -8.1 \pm 0.3$, $n = 9$; $V_h = -48.2 \pm 0.7$, $n = 7$). (*B*) Semilogarithmic plot of the fast time constants for each mutant as described in Fig. 2. (*Inset*) The data at positive voltages plotted on a linear scale.

The CT Determines the Difference in Rate of Inactivation Between Brain and Cardiac Na$^+$ Channels. Substituting the cardiac CT in the brain Na$^+$ channel transfers cardiac inactivation kinetics to the brain channel as observed for chimera Na$_v$1.2/1.5CT. Similarly, substituting the brain Na$_v$1.2a CT in the cardiac Na$_v$1.5 channel transfers brain inactivation kinetics to the cardiac channel, as observed for chimera Na$_v$1.5/1.2CT. Thus, the CT is responsible for the faster inactivation of Na$_v$1.2a brain channels relative to cardiac Na$^+$ channels.

The CT Has an Important Influence on the Voltage Dependence of Inactivation. The CTs of Na$_v$1.2a and Na$_v$1.5 have a parallel influence on rate of inactivation and on the steady-state inactivation curves. Evidently, inactivation is enhanced in two ways by substitution of the Na$_v$1.2a CT: increased rate of inactivation from the open state and increased steady-state inactivation from the closed states. The CT of the cardiac channel has opposite effects. However, these effects of the CTs magnify the already large difference in steady-state inactivation between brain and cardiac sodium channels rather than exchanging the properties of the two channels. Therefore, the CTs greatly influence steady-state inactivation, but other molecular features of these two channel types are responsible for their different voltage dependences of steady-state inactivation.

Although the CT of Na$_v$1.2a causes stronger inactivation than its cardiac counterpart, the separation between the midpoint voltages of the activation and inactivation is virtually identical, indicating similar efficiency of coupling of activation to inactivation (Fig. 3). This comparison also supports the conclusion that other parts of these two channels determine the strength of coupling of activation to inactivation, thereby conserving the voltage separation between activation and inactivation curves.

The CT Favors Inactivation. When the distal CT is truncated, inactivation from the open state during strong depolarizations is accelerated, and the steady-state inactivation curve is shifted toward more negative membrane potentials. Thus, the distal CT normally inhibits inactivation. Detailed deletion analysis of the distal C terminal of the brain Na$_v$1.2a channel indicated that this net effect resulted from at least two distinct determinants that inhibited inactivation. Deleting only the final eight amino acid residues in the CT caused a pronounced acceleration of inactivation, which was almost as strong as that caused by truncation of the entire tail. These final eight amino acid residues must normally slow inactivation. Further deletion between residues 1951 and 1891 gave even stronger inactivation, indicating that amino acid residues in this region have an additional inhibitory effect on inactivation. This net inhibitory effect of the distal half of the CT results from the sum of interactions opposing inactivation.

Role of the Membrane Proximal Half of the CT in Inactivation. The effects of deleting the distal half of the CT of either the brain Na$_v$1.2a or the cardiac Na$_v$1.5 channel are smaller than the effects of exchanging the entire lengths of the tails. Replacing the entire cardiac CT with that of the brain channel caused a 15-mV negative shift in steady-state inactivation. The effects of truncating the distal halves of the C termini of the brain and cardiac channels differed by only 3 mV. Assuming that these effects are additive, −12 mV of the −15-mV shift caused by exchanging CTs is caused by transfer of the membrane-proximal half of the CT. The converse experiment, replacing the CT of the brain channel with that of the cardiac channel, resulted in a +12 mV shift in the steady-state inactivation curve. Of this, 3 mV might be attributed to differential effects of the distal halves of the Na$_v$1.2a and Na$_v$1.5 CTs. The remaining 9 mV must be attributed to differences in the membrane-proximal portion. Thus, 9- to 12-mV of the shifts of steady-state inactivation of the brain versus cardiac Na$^+$ channels can likely be attributed to the membrane proximal halves of the CTs.

For both the brain and cardiac Na$^+$ channels, truncating the CT caused a 1.3- to 1.4-fold increase in the rate of inactivation. In contrast, substituting the Na$_v$1.2a CT in the cardiac channel caused a 1.9-fold increase in the rate of inactivation, while substituting the cardiac CT in the brain channel reduced the rate of inactivation of the brain channel 2-fold. Thus, the membrane-proximal halves of the CTs are likely to have larger effects on both the kinetics and voltage dependence of inactivation.

Molecular Mechanism of Action of the CT in Inactivation. There are multiple steps in the pathway leading to inactivation of Na$^+$ channels. Channel activation occurs first. It is thought to involve molecular rearrangements in the transmembrane segments of all four homologous domains. These rearrangements link to conformational changes near the extracellular side of homologous domains III and IV (35). Blocking these movements of extracellular loops with toxins (36, 37) or mutations (38) slows channel inactivation. Furthermore, mutations in these extracellular regions appear to prevent coupling of activation to inactivation (38). These movements at the extracellular surface of the

Na^+ channel are molecularly linked to additional conformational changes on the intracellular face of the channel. The structure responsible for the last step in fast inactivation is the intracellular loop between domain III and IV (L_{III-IV}) (10, 12, 39), which moves during the inactivation process (13, 40) and blocks conduction through the pore of the channel (41). L_{III-IV} is thought to act by binding to a receptor region on the intracellular surface of the channel. Candidates for forming the receptor site for L_{III-IV} include the intracellular loops connecting transmembrane segments S4 and S5 in domains III and IV (42–44). The intracellular end of transmembrane segment IVS6 also appears to play an important role (45).

Although the inactivation gate formed by L_{III-IV} ultimately is responsible for inactivation, it is unable to transfer the inactivation properties to the cardiac sodium channel (14, 46). Thus, another region of the channel must modulate its movement, resulting in altered inactivation. Our results suggest that the CT performs this function. Single-channel comparison of inactivation in brain and cardiac channels reveals bursts of openings that are prolonged in cardiac channels, indicating slowed entry into the inactivated state (9, 47). Our data show that these effects require the CT of the channel. The CT could modulate inactivation by interacting directly with the structures involved in the inactivation process. For example, the CT could interact with L_{III-IV}, in this way modulating the kinetics of its closure. Similarly, the CT could interact with the IIIS4–S5 loop, the IVS4–S5 loop, or the intracellular end of the IVS6 segment and slow their formation of an effective inactivation gate receptor. Alternatively, the CT could exert its effects through allosteric coupling, caused by short or long-range interactions. Further analysis of mutations in the CT that alter inactivation may allow distinction among these possible mechanisms.

We thank Elizabeth M. Sharp for making the mutant $Na_v1.5$-K1888. This study was supported by Human Frontier Science Program Fellowship LT-613/98 (to M.M.), a Canadian Institutes of Health Research Fellowship (to F.H.Y.), and National Institutes of Health Grant NS34801 (to T.S.).

1. Hodgkin, A. L. & Huxley, A. F. (1952) *J. Physiol. (London)* **117**, 500–544.
2. Fozzard, H. A. & Hanck, D. A. (1996) *Physiol. Rev.* **76,** 887–926.
3. Marban, E., Yamagishi, T. & Tomaselli, G. (1998) *J. Physiol. (London)* **508,** 647–657.
4. Catterall, W. A. (2000) *Neuron* **26,** 13–25.
5. Lehmann-Horn, F. & Jurkat-Rott, K. (1999) *Physiol. Rev.* **79,** 1317–1372.
6. Goldin, A. L. (2001) *Annu. Rev. Physiol.* **63,** 871–894.
7. Noda, M., Ikeda, T., Suzuki, H., Takeshima, H., Takahashi, T., Kuno, M. & Numa, S. (1986) *Nature (London)* **322,** 826–828.
8. Gordon, D., Merrick, D., Auld, V., Dunn, R., Goldin, A. L., Davidson, N. & Catterall, W. A. (1987) *Proc. Natl. Acad. Sci. USA* **84,** 8682–8686.
9. Kirsch, G. E. & Brown, A. M. (1989) *J. Gen. Physiol.* **93,** 85–99.
10. Vassilev, P. M., Scheuer, T. & Catterall, W. A. (1988) *Science* **241,** 1658–1661.
11. Vassilev, P., Scheuer, T. & Catterall, W. A. (1989) *Proc. Natl. Acad. Sci. USA* **86,** 8147–8151.
12. Stühmer, W., Conti, F., Suzuki, H., Wang, X. D., Noda, M., Yahagi, N., Kubo, H. & Numa, S. (1989) *Nature (London)* **339,** 597–603.
13. Kellenberger, S., Scheuer, T. & Catterall, W. A. (1996) *J. Biol. Chem.* **271,** 30971–30979.
14. Hartmann, H. A., Tiedeman, A. A., Chen, S. F., Brown, A. M. & Kirsch, G. E. (1994) *Circ. Res.* **75,** 114–122.
15. Wehrens, X. H., Abriel, H., Cabo, C., Benhorin, J. & Kass, R. S. (2000) *Circulation* **102,** 584–590.
16. Veldkamp, M. W., Viswanathan, P. C., Bezzina, C., Baartscheer, A., Wilde, A. A. & Balser, J. R. (2000) *Circ. Res.* **86,** E91–E97.
17. Lupoglazoff, J. M., Cheav, T., Baroudi, G., Berthet, M., Denjoy, I., Cauchemez, B., Extramiana, F., Chahine, M. & Guicheney, P. (2001) *Circ. Res.* **89,** E16–E21.
18. Baroudi, G. & Chahine, M. (2000) *FEBS Lett.* **487,** 224–228.
19. Baroudi, G., Carbonneau, E., Pouliot, V. & Chahine, M. (2000) *FEBS Lett.* **467,** 12–16.
20. Rivolta, I., Abriel, H., Tateyama, M., Liu, H., Memmi, M., Vardas, P., Napolitano, C., Priori, S. G. & Kass, R. S. (2001) *J. Biol. Chem.* **276,** 30623–30630.
21. Qu, Y., Rogers, J., Tanada, T., Scheuer, T. & Catterall, W. A. (1995) *Proc. Natl. Acad. Sci. USA* **92,** 11839–11843.
22. Linford, N. J., Cantrell, A. R., Qu, Y., Scheuer, T. & Catterall, W. A. (1998) *Proc. Natl. Acad. Sci. USA* **95,** 13947–13952.
23. Herlitze, S., Garcia, D. E., Mackie, K., Hille, B., Scheuer, T. & Catterall, W. A. (1996) *Nature (London)* **380,** 258–262.
24. Margolskee, R. F., McHendry-Rinde, B. & Horn, R. (1993) *BioTechniques* **15,** 906–911.
25. Ma, J. Y., Catterall, W. A. & Scheuer, T. (1997) *Neuron* **19,** 443–452.
26. Auld, V. J., Goldin, A. L., Krafte, D. S., Marshall, J., Dunn, J. M., Catterall, W. A., Lester, H. A., Davidson, N. & Dunn, R. J. (1988) *Neuron* **1,** 449–461.
27. Auld, V. J., Goldin, A. L., Krafte, D. S., Catterall, W. A., Lester, H. A., Davidson, N. & Dunn, R. J. (1990) *Proc. Natl. Acad. Sci. USA* **87,** 323–327.
28. Rogart, R. B., Cribbs, L. L., Muglia, L. K., Kephart D. A. & Kaiser, M. W. (1989) *Proc. Natl. Acad. Sci. USA* **86,** 8170–8174.
29. White, M. M., Chen, L. Q., Kleinfield, R., Kallen, R. G. & Barchi, R. L. (1991) *Mol. Pharmacol.* **39,** 604–608.
30. Qu, Y., Rogers, J., Tanada, T., Scheuer, T. & Catterall, W. A. (1994) *Proc. Natl. Acad. Sci. USA* **91,** 3289–3293.
31. Kellenberger, S., West, J. W., Scheuer, T. & Catterall, W. A. (1997) *J. Gen. Physiol.* **109,** 589–605.
32. Kellenberger, S., West, J. W., Catterall, W. A. & Scheuer, T. (1997) *J. Gen. Physiol.* **109,** 607–617.
33. Cummins, T. R., Zhou, J., Sigworth, F. J., Ukomadu, C., Stephan, M., Ptacek, L. J. & Agnew, W. S. (1993) *Neuron* **10,** 667–678.
34. Ukomadu, C., Zhou, J., Sigworth, F. J. & Agnew, W. S. (1992) *Neuron* **8,** 663–676.
35. Cha, A., Ruben, P. C., George, A. L., Jr., Fujimoto, E. & Bezanilla, F. (1999) *Neuron* **22,** 73–87.
36. Rogers, J. C., Qu, Y., Tanada, T. N., Scheuer, T. & Catterall, W. A. (1996) *J. Biol. Chem.* **271,** 15950–15962.
37. Benzinger, G. R., Kyle, J. W., Blumenthal, K. M. & Hanck, D. A. (1998) *J. Biol. Chem.* **273,** 80–84.
38. Chahine, M., George, A. L., Jr., Zhou, M., Ji, S., Sun, W., Barchi, R. L. & Horn, R. (1994) *Neuron* **12,** 281–294.
39. West, J. W., Patton, D. E., Scheuer, T., Wang, Y., Goldin, A. L. & Catterall, W. A. (1992) *Proc. Natl. Acad. Sci. USA* **89,** 10910–10914.
40. Vedantham, V. & Cannon, S. C. (1998) *J. Gen. Physiol.* **111,** 83–93.
41. Eaholtz, G., Scheuer, T. & Catterall, W. A. (1994) *Neuron* **12,** 1041–1048.
42. Lerche, H., Peter, W., Fleischhauer, R., PikaHartlaub, U., Malina, T., Mitrovic, N. & Lehmann-Horn, F. (1997) *J. Physiol. (London)* **505,** 345–352.
43. Smith, M. R. & Goldin, A. L. (1997) *Biophys. J.* **73,** 1885–1895.
44. McPhee, J. C., Ragsdale, D. S., Scheuer, T. & Catterall, W. A. (1998) *J. Biol. Chem.* **273,** 1121–1129.
45. McPhee, J. C., Ragsdale, D. S., Scheuer, T. & Catterall, W. A. (1995) *J. Biol. Chem.* **270,** 12025–12034.
46. Makita, N., Bennett, P. B., Jr. & George, A. L. Jr. (1996) *Circ. Res.* **78**, 244–252.
47. Berman, M. F., Camardo, J. S., Robinson, R. B. & Siegelbaum, S. A. (1989) *J. Physiol. (London)* **415,** 503–531.